Pair-breaking in superconductors with strong spin-orbit coupling

D. C. Cavanagh,[1] Daniel F. Agterberg,[2,*] and P. M. R. Brydon[3,†]

[1] *Department of Physics, University of Otago, P.O. Box 56, Dunedin 9054, New Zealand*
[2] *Department of Physics, University of Wisconsin, Milwaukee, Wisconsin 53201, USA*
[3] *Department of Physics and MacDiarmid Institute for Advanced Materials and Nanotechnology, University of Otago, P.O. Box 56, Dunedin 9054, New Zealand*

(Dated: July 4, 2022)

We study the influence of symmetry-breaking perturbations on superconductivity in multiorbital materials, with a particular focus on an external magnetic field. We introduce the field-fitness function which characterizes the pair-breaking effects of the perturbation on a given superconducting state. For even parity superconductors we find that this field-fitness function for an external magnetic field is one, implying that the paramagnetic response is controlled only by a generalized effective g-factor. For odd parity superconductors, the interplay of the effective g-factor and the field-fitness function can lead to counter-intuitive results. We demonstrate this for p-wave pairing in the effective $j = 3/2$ electronic states of the Luttinger-Kohn model.

arXiv:2207.01191v1 [cond-mat.supr-con] 4 Jul 2022

Introduction. A diverse variety of superconductors have recently been found to exhibit critical fields far exceeding the Pauli limiting field, e.g. UTe_2 [1], $CeRh_2As_2$ [2], UCoGe[3], URhGe[3], and $YbRh_2Si_2$ [4]. In some of these materials superconductivity even appears as a reentrant phase [1, 3], again far above the Pauli field. The origin of this anomalous high-field behaviour has been attributed to spin-triplet superconductivity. However, the fermiology of these materials is complicated, with multiple bands crossing the Fermi surface. Moreover, spin-orbit coupling is expected to be large due to the presence of heavy elements. Due to the interplay of the normal-state band structure, the structure of the odd-parity pairing potential, and the applied magnetic field, it is not clear that the established theory for the magnetic response of a triplet superconductor is applicable [5, 6].

Concurrent to these experimental developments, it has been realized that internal degrees of freedom of the band electrons, e.g. sublattice or orbital, can profoundly impact the magnetic response of even-parity superconductors. In particular, the large critical fields observed in artificial Rashba heterostructures [7, 8], $CeRh_2As_2$ [2, 9], and WTe_2 [10] are believed to arise from a "hidden" antisymmetric spin-orbit coupling (ASOC) [11]. This ASOC is odd in momentum and has opposite signs for internal degrees of freedom that are related by inversion symmetry (IS). This preserves IS and the two-fold degeneracy of the band electron states. Similar to noncentrosymmetric materials, [12] however, the ASOC reduces the Zeeman splitting of the band states and so enhances the Pauli limit [13]. For odd-parity superconductivity, however, the effect of the ASOC on the critical fields is not as well explored. However, in one remarkable example, $CeRh_2As_2$, spin-singlet pairing interactions give way to extremely high critical fields due to the formation of an odd-parity superconducting state that is stabilized by the ASOC [2, 14].

There also exist materials where a symmetric spin-orbit coupling (SSOC), i.e. the spin-orbit coupling is even in momentum, is important. This influence of this SSOC on superconductivity has been studied in the context of the iron pnictides [15], Sr_2RuO_4 [16, 17], half-Heusler materials, [18, 19] and the pyrochlore lattice [20]. The latter two cases support effective $j = 3/2$ electronic states which exhibit properties that are quite different from the more usual $j = 1/2$ states [21]. The magnetic response of even-parity superconducting states in such materials shows similar features to the case of the ASOC [22]; the response of odd-parity superconductivity also remains poorly understood. Indeed, one of the main results of this work is to reveal the counter-intuitive response of odd-parity states in $j = 3/2$ materials to applied fields.

In this article we examine the influence of the spin-orbit coupling on the response of a superconducting state to a perturbation which breaks either IS or time-reversal symmetry (TRS), with a focus on the familiar example of an applied magnetic field. Within a general minimal model for systems with both antisymmetric and symmetric spin-orbit coupling, we show that the response of the superconducting state to the perturbation is fully determined by two basis-independent quantities: a generalized effective g-factor, and a parameter that quantifies the pair-breaking due to the field, which we term the field-fitness function F_h by analogy with the superconducting fitness [16, 23]. In the case of an external magnetic field, these quantities also control the spin susceptibility in the superconducting state. For even-parity superconductors, $F_h = 1$, so that the response is given solely by the effective g-factor; in contrast, odd-parity superconducting states display a complicated interplay of the field-fitness and the effective g-factor. We apply our general theory to odd-parity superconductivity in $j = 3/2$ materials, where we find that the SSOC leads to a magnetic response very unlike that of $j = 1/2$ superconductors.

General theory. We consider a system described by the

* agterber@uwm.edu
† philip.brydon@otago.ac.nz

Bogoliubov-de Gennes Hamiltonian

$$H = \sum_{\boldsymbol{k}} \vec{\Psi}_{\boldsymbol{k}}^{\dagger} \begin{pmatrix} \mathcal{H}_{0,\boldsymbol{k}} & \Delta_{\boldsymbol{k}} \\ \Delta_{\boldsymbol{k}}^{\dagger} & -\mathcal{H}_{0,-\boldsymbol{k}}^{T} \end{pmatrix} \vec{\Psi}_{\boldsymbol{k}}, \tag{1}$$

where $\vec{\Psi}_{\boldsymbol{k}} = (\vec{c}_{\boldsymbol{k}}, \vec{c}_{-\boldsymbol{k}}^{\dagger})$, with $\vec{c}_{\boldsymbol{k}}$ representing a spinor of annihilation operators for fermions with four internal degrees of freedom. In the presence of both TRS and IS, the most general form of the Hamiltonian matrix $\mathcal{H}_{0,\boldsymbol{k}}$ is [24, 25]

$$\mathcal{H}_{0,\boldsymbol{k}} = \varepsilon_{0,\boldsymbol{k}}\mathbb{1} + \vec{\varepsilon}_{\boldsymbol{k}} \cdot \vec{\gamma} = \varepsilon_{0,\boldsymbol{k}}\mathbb{1} + \bar{\mathcal{H}}_{0,\boldsymbol{k}}, \tag{2}$$

where $\vec{\gamma} = (\gamma^1, \gamma^2, \gamma^3, \gamma^4, \gamma^5)$ are the mutually anticommuting Euclidean Dirac matrices with coefficients $\vec{\varepsilon}_{\boldsymbol{k}} = (\varepsilon_{1,\boldsymbol{k}}, \varepsilon_{2,\boldsymbol{k}}, \varepsilon_{3,\boldsymbol{k}}, \varepsilon_{4,\boldsymbol{k}}, \varepsilon_{5,\boldsymbol{k}})$. The Hamiltonian has doubly-degenerate eigenenergies $\xi_{\pm,\boldsymbol{k}} = \varepsilon_{0,\boldsymbol{k}} \pm |\vec{\varepsilon}_{\boldsymbol{k}}|$, where $|\vec{\varepsilon}_{\boldsymbol{k}}| = \sqrt{\sum_{l=1}^{5} \varepsilon_{l,\boldsymbol{k}}^2}$. In Eq. 2 we have introduced $\bar{\mathcal{H}}_{0,\boldsymbol{k}} = \vec{\epsilon}_{\boldsymbol{k}} \cdot \vec{\gamma}$ to denote the part of the Hamiltonian which depends nontrivially on the internal degrees of freedom.

Hamiltonians with the form of Eq. 2 describe a diverse range of two-band systems [10, 14, 15, 18, 24, 26–29], and so the exact form of the γ matrices depends on the system under consideration [30]. For spin-$\frac{1}{2}$ systems, we generally construct the γ matrices as Kronecker products of Pauli matrices acting in the orbital and spin spaces. In this case we choose γ^1 and γ^2 to be trivial in the spin space, with these contributions to the Hamiltonian describing purely orbital effects, while the remaining matrices couple the spin and orbital degrees of freedom, accounting for SOC in the system. As we shall see, this parameterization is also valid for spin-$\frac{3}{2}$ systems, even though the underlying orbital and spin degrees of freedom cannot be factorized.

The pairing potential appearing in Eq. 1 is written $\Delta_{\boldsymbol{k}} = \Delta_0 \tilde{\Delta}_{\boldsymbol{k}} U_T$, where Δ_0 is the magnitude, $\tilde{\Delta}_{\boldsymbol{k}}$ encodes the dependence on the momentum and the internal degrees of freedom, and U_T is the unitary part of the time-reversal operator. The general form for even- (e) and odd-parity (o) states is

$$\tilde{\Delta}_{\boldsymbol{k}}^{(e)} = \sum_{a=0}^{5} e_{\boldsymbol{k}}^{a} \gamma^a \tag{3}$$

$$\tilde{\Delta}_{\boldsymbol{k}}^{(o)} = \sum_{a=1}^{4} \sum_{b>a} o_{\boldsymbol{k}}^{ab} i\gamma^a\gamma^b \tag{4}$$

where $e_{\boldsymbol{k}}^{a}$ and $o_{\boldsymbol{k}}^{ab}$ are normalized form factors. Note that only when the internal degrees of freedom transform trivially under inversion are the functions $e_{\boldsymbol{k}}^{a}$ and $o_{\boldsymbol{k}}^{ab}$ necessarily even and odd in momentum, respectively.

Due to the mixing of orbital and spin, the pairing potential in the band basis typically has both intraband and interband matrix elements. The intraband gap is particularly important as it is responsible for the Cooper instability. Assuming that Δ_0 is small compared to the band separation, the gap in band a is given by

$$|\Delta_{a,\boldsymbol{k}}|^2 = \Delta_0^2 \frac{\mathrm{Tr}\{|\{\bar{\mathcal{H}}_{0,\boldsymbol{k}}, \tilde{\Delta}_{\boldsymbol{k}}\}|^2 \mathcal{P}_{a,\boldsymbol{k}}\}}{8\,|\vec{\varepsilon}_{\boldsymbol{k}}|^2}, \tag{5}$$

where $\{\bar{\mathcal{H}}_{0,\boldsymbol{k}}, \tilde{\Delta}_{\boldsymbol{k}}\} U_T = F_A$ is the superconducting fitness as defined in Refs. [16, 23], and $\mathcal{P}_{a,\boldsymbol{k}} = \frac{1}{2}(\mathbb{1} + a\bar{\mathcal{H}}_{0,\boldsymbol{k}}/|\vec{\epsilon}|)$ projects into the $a = \pm$ band. The projection operator is necessary to account for band-dependence of the intraband pairing, which can arise when $\tilde{\Delta}_{\boldsymbol{k}}\tilde{\Delta}_{\boldsymbol{k}}^{\dagger} \not\propto \mathbb{1}$.

To investigate the effect of symmetry-breaking, we introduce the perturbation Hamiltonian

$$\delta H = \sum_{\boldsymbol{k}} \vec{\Psi}_{\boldsymbol{k}}^{T} \begin{pmatrix} \mathcal{H}_{h,\boldsymbol{k}} & 0 \\ 0 & -\mathcal{H}_{h,-\boldsymbol{k}}^{T} \end{pmatrix} \vec{\Psi}_{\boldsymbol{k}}. \tag{6}$$

We adopt a general form of $\mathcal{H}_{h,\boldsymbol{k}}$

$$\mathcal{H}_{h,\boldsymbol{k}} = \sum_{\alpha=0}^{5} h_{0\alpha,\boldsymbol{k}} \gamma^{\alpha} + \sum_{\alpha=1}^{4} \sum_{\beta>\alpha} h_{\alpha\beta,\boldsymbol{k}} i\gamma^{\alpha}\gamma^{\beta}, \tag{7}$$

The perturbation lifts the twofold degeneracy of the normal state spectrum: For sufficiently well-separated bands, the perturbed energies of band a are $\xi_{a,\pm,\boldsymbol{k}} \approx \xi_{a,\boldsymbol{k}} \pm \tilde{g}_{a,\boldsymbol{k}} h_{\boldsymbol{k}}$, where $h_{\boldsymbol{k}}^2 = \sum_{\alpha,\beta} h_{\alpha\beta,\boldsymbol{k}}^2 = \mathrm{Tr}\{|\mathcal{H}_{h,\boldsymbol{k}}|^2\}/4$, and the effective g-factor in band a is

$$\tilde{g}_{a,\boldsymbol{k}}^2 = \frac{\mathrm{Tr}\{|\{\bar{\mathcal{H}}_{0,\boldsymbol{k}}, \mathcal{H}_{h,\boldsymbol{k}}\}|^2 \mathcal{P}_{a,\boldsymbol{k}}\}}{8\,|\vec{\varepsilon}_{\boldsymbol{k}}|^2\, h_{\boldsymbol{k}}^2}. \tag{8}$$

Equation 8 resembles the expression for the intraband superconducting gap Eq. 5, and can be similarly interpreted as giving the splitting of the bands due to the projection of the perturbation onto band a. When $|\mathcal{H}_{h,\boldsymbol{k}}|^2 \propto \mathbb{1}$ the splitting of the energy spectrum is independent of the band index, i.e. $g_{a,\boldsymbol{k}} = g_{\boldsymbol{k}}$; more generally, when $|\mathcal{H}_{h,\boldsymbol{k}}|^2 \not\propto \mathbb{1}$ the effective g-factors are different in each band, which is accounted for by the projection operator in Eq. 8. For definiteness, in the following we consider only perturbations which break TRS but preserve IS; the results for perturbations which break IS but preserve TRS are similar and provided in appendix A 4.

Pair-breaking. The lifting of the two-fold degeneracy of the band states by the perturbation generally suppresses the superconductivity. The central result of our work is that the pair-breaking effects of the perturbation in band a can be quantified by the *field-fitness function*

$$\tilde{F}_{h,\boldsymbol{k}}^{(a)} = \frac{\mathrm{Tr}\{|\{\{\bar{\mathcal{H}}_{0,\boldsymbol{k}}, \tilde{\Delta}_{\boldsymbol{k}}\}, \{\bar{\mathcal{H}}_{0,\boldsymbol{k}}, \mathcal{H}_{h,\boldsymbol{k}}\}\}|^2 \mathcal{P}_{a,\boldsymbol{k}}\}}{2\mathrm{Tr}\{|\{\bar{\mathcal{H}}_{0,\boldsymbol{k}}, \mathcal{H}_{h,\boldsymbol{k}}\}|^2 \mathcal{P}_{a,\boldsymbol{k}}\}\mathrm{Tr}\{|\{\bar{\mathcal{H}}_{0,\boldsymbol{k}}, \tilde{\Delta}_{\boldsymbol{k}}\}|^2 \mathcal{P}_{a,\boldsymbol{k}}\}}. \tag{9}$$

The field-fitness function ranges in value from zero to one. For $\tilde{F}_{h,\boldsymbol{k}}^{(a)} = 0$, the states at $\boldsymbol{k}$ and $-\boldsymbol{k}$ involved in the intraband pairing remain degenerate, and so there is no pair-breaking effect. On the other hand, the perturbation is maximally pair-breaking for $\tilde{F}_{h,\boldsymbol{k}}^{(a)} = 1$, i.e. the states paired by the intraband pairing potential are split by the

perturbation. An intermediate value $0 < \tilde{F}^{(a)}_{h,\boldsymbol{k}} < 1$ indicates that the intraband pairing potential pairs electrons in a superposition of the perturbed states, and there will be some pair-breaking effect. Inserting Eq. 3 into Eq. 9, we find that for any even-parity state the field fitness $\tilde{F}^{(a)}_{h,\boldsymbol{k}} = 1$, as the numerator can be factored to give the denominator. Since even-parity superconductors always pair time-reversed partners within the same band, any TRS-breaking perturbation is maximally pair-breaking. On the other hand, odd-parity superconducting states do not necessarily pair time-reversed states in the same band, and so they may experience less or no pair-breaking due to broken TRS, i.e. $0 \leq \tilde{F}^{(a)}_{h} \leq 1$.

Solving the linearized gap equation in the presence of the TRS-breaking perturbation gives the critical temperature T_c in terms of the unperturbed value $T_{c,0}$,

$$\log\left(\frac{T_c}{T_{c,0}}\right) = \sum_{a=\pm}\left\langle\left[\frac{\mathcal{D}_{a,\boldsymbol{k}}\left|\Delta_{a,\boldsymbol{k}}\right|^2}{\sum_{a'=\pm}\langle\mathcal{D}_{a',\boldsymbol{k}'}\left|\Delta_{a',\boldsymbol{k}'}\right|^2\rangle_{a'}}\right]\tilde{F}^{(a)}_{h,\boldsymbol{k}}\mathrm{Re}\left\{\psi\left(\frac{1}{2}\right)-\psi\left(\frac{1}{2}+i\frac{\tilde{g}_{a,\boldsymbol{k}}h_{\boldsymbol{k}}}{2\pi k_B T_c}\right)\right\}\right\rangle_a, \tag{10}$$

where $\psi(x)$ is the digamma function, $\langle\ldots\rangle_a$ indicates the average over the Fermi surface of band a, $\mathcal{D}_{a,\boldsymbol{k}} = |\vec{\nabla}_{\boldsymbol{k}}\xi_{a,\boldsymbol{k}}|^{-1}$, and the factor in the square brackets defines the fraction of the total condensation energy due to the gap on each band. The suppression of the critical temperature by a TRS-breaking perturbation is controlled by both the field fitness function and the effective g-factor, which tune the degree of pair-breaking and the magnitude of the band splitting, respectively. A brief derivation of Eq. 10 is presented in appendix A.

Magnetic susceptibility. We now turn to the important case where the perturbation is an applied magnetic field, which couples to the electron states via the Zeeman effect. A key experimental quantity is the magnetic susceptibility, which in a multiband system can be divided into components due to intraband ('Pauli') and interband ('van Vleck') transitions. The latter is negligibly affected by superconductivity, as the pairing potential is typically much smaller than the band separation. On the other hand, the Pauli contribution carries clear signatures of the pair-breaking effect. For a field applied along the i-axis, the Pauli susceptibility below the critical temperature is given by

$$\chi_{ii} = \sum_{a=\pm}\left\langle 2\mu_B^2\mathcal{D}_{a,\boldsymbol{k}}\tilde{g}^{(i)\,2}_{a,\boldsymbol{k}}\left\{1+\tilde{F}^{(a)}_{i,\boldsymbol{k}}\left[Y_a(\hat{k},T)-1\right]\right\}\right\rangle_a, \tag{11}$$

where $\tilde{g}^{(i)}_{a,\boldsymbol{k}}$ is the effective g-factor for an i-axis field, and $Y_a(\hat{k},T)$ is the angle-dependent Yosida function for the intraband gap Eq. 5. Explicit expressions for the susceptibility in both the normal and superconducting states are provided in the appendix A. For even-parity gaps $\tilde{F}^{(a)}_{h,\boldsymbol{k}} = 1$, and the pairing suppresses the Pauli susceptibility, with it vanishing at zero temperature. On the other hand, an odd-parity state typically gives only a partial suppression of the Pauli susceptibility; In the extreme case $\tilde{F}^{(a)}_{h,\boldsymbol{k}} = 0$ the susceptibility is unaffected by the superconductivity.

$j = \frac{3}{2}$ *superconductors.* As a concrete application of our approach we consider a system of electrons with an effective $j = \frac{3}{2}$. A minimal model is given by the Luttinger-Kohn Hamiltonian

$$\mathcal{H}_{0,\boldsymbol{k}} = \left(\alpha\left|\boldsymbol{k}\right|^2-\mu\right)\mathbb{1}+\beta_1\sum_i k_i^2 J_i+\beta_2\sum_{i'\neq i}k_i k_{i'}J_iJ_{i'}, \tag{12}$$

where J_i are the spin-$\frac{3}{2}$ matrices and the indices i, i' run over Cartesian coordinates. The Hamiltonian can be cast into the form of Eq. 2 by defining the γ matrices $\vec{\gamma} = (\frac{1}{\sqrt{3}}[J_x^2-J_y^2], \frac{1}{3}[2J_z^2-J_x^2-J_y^2], \frac{1}{\sqrt{3}}\{J_y,J_z\}, \frac{1}{\sqrt{3}}\{J_x,J_y\}, \frac{1}{\sqrt{3}}\{J_x,J_z\})$, with corresponding coefficients $\vec{\varepsilon} = (\sqrt{3}\beta_1(k_x^2-k_y^2)/2, \sqrt{3}\beta_1(3k_z^2-|\boldsymbol{k}|^2)/2, \sqrt{3}\beta_2 k_y k_z, \sqrt{3}\beta_2 k_x k_y, \sqrt{3}\beta_2 k_x k_z)$. The strong SOC in the Luttinger-Kohn model leads to a pronounced spin-momentum locking. This is most clearly observed in the limit $\beta_1 = \beta_2$, where the model has full spherical symmetry and the quantity $\boldsymbol{k}\cdot\mathbf{J}$ commutes with the Hamiltonian, i.e. the projection of the spin along $\boldsymbol{k}$ is a good quantum number. The eigenstates are classified by the "helical" index σ such that $\hat{\boldsymbol{k}}\cdot\mathbf{J}|\sigma\rangle_{\boldsymbol{k}} = \sigma|\sigma\rangle_{\boldsymbol{k}}$, defining a spin-$\frac{3}{2}$ band ($\sigma = \pm\frac{3}{2}$) and spin-$\frac{1}{2}$ band ($\sigma = \pm\frac{1}{2}$). This argument remains valid along high-symmetry directions in the presence of cubic anisotropy, allowing us to identify spin-$\frac{1}{2}$ and -$\frac{3}{2}$ bands when $\beta_1 \neq \beta_2$. As we will show below, compared to the spin-$\frac{1}{2}$-band, the spin-$\frac{3}{2}$ band exhibits counter-intuitive properties.

The spin-momentum locking produces a highly anisotropic Zeeman splitting of the bands by an applied magnetic field $H_h = g\mu_B\boldsymbol{h}\cdot\mathbf{J}$. Although the general result using Eq. 8 is complicated, in the rotationally-symmetric limit the effective g-factors take the compact forms $\tilde{g}_{1/2} = \sqrt{1-3|\hat{\boldsymbol{h}}\cdot\hat{\boldsymbol{k}}|^2/4}$ and $\tilde{g}_{3/2} = 3|\hat{\boldsymbol{h}}\cdot\hat{\boldsymbol{k}}|/2$ in the spin-$\frac{1}{2}$ and -$\frac{3}{2}$ bands, respectively; these effective g-factors remain approximately valid in the general case. Note that there is no splitting of the spin-$\frac{3}{2}$ band in the direction perpendicular to the field, whereas the splitting of the spin-$\frac{1}{2}$ states is maximal in this plane. To understand this, we introduce the momentum-dependent angular momentum operators $J^{\boldsymbol{k}}_z = \hat{\boldsymbol{k}}\cdot\mathbf{J}$, and raising and lowering operators $J^{\boldsymbol{k}}_\pm$ which satisfy $[J^{\boldsymbol{k}}_z, J^{\boldsymbol{k}}_\pm] = \pm J^{\boldsymbol{k}}_\pm$. The band states are eigenstates of $J^{\boldsymbol{k}}_z$, i.e. $J^{\boldsymbol{k}}_z|\sigma\rangle_{\boldsymbol{k}} = \sigma|\sigma\rangle_{\boldsymbol{k}}$,

and the action of the raising and lowering operators is $J^{\boldsymbol{k}}_{\pm}|\sigma\rangle_{\boldsymbol{k}} = \sqrt{(\frac{3}{2}\mp\sigma)(\frac{3}{2}\pm\sigma+1)}|\sigma\pm1\rangle_{\boldsymbol{k}}$. Expressing the Zeeman Hamiltonian in terms of these operators we have $H_h = g\mu_B\left(\mathbf{h}\cdot\hat{\boldsymbol{k}}J^{\boldsymbol{k}}_z + h^{\boldsymbol{k}}_+ J^{\boldsymbol{k}}_+ + h^{\boldsymbol{k}}_- J^{\boldsymbol{k}}_-\right)$; the functions $h^{\boldsymbol{k}}_{\pm} = -h^{-\boldsymbol{k}}_{\pm}$ are vanishing for $\hat{\boldsymbol{k}} \parallel \mathbf{h}$ and take maximal magnitude in the plane perpendicular to $\boldsymbol{k}$; explicit expressions are given in the appendix B. Since the raising and lowering operators do not couple the $\sigma = \pm\frac{3}{2}$ states, this immediately explains why there is no splitting for $\boldsymbol{k} \perp \mathbf{h}$ in the spin-$\frac{3}{2}$ band; conversely, the larger matrix elements for the raising and lowering operators compared to the z-spin operator gives a maximum of the Zeeman splitting for the spin-$\frac{1}{2}$ band in this plane.

The spin-momentum locking also profoundly influences the superconducting gap structure, which we illustrate by two odd-parity states: the fully-gapped p-wave triplet A_{1u} state with $\tilde{\Delta}_{1u} = \frac{2}{\sqrt{5}}(\boldsymbol{k}\cdot\mathbf{J})U_T$, and a nodal p-wave septet A_{2u} state $\tilde{\Delta}_{2u} = \frac{1}{\sqrt{3}}(\boldsymbol{k}\cdot\mathbf{T})U_T$, where $T_i = \{J_i, J^2_{i+1} - J^2_{i+2}\}$ for i defined cyclically (e.g. $J_{y+2} = J_x$). These two states are the leading p-wave instabilities in the spin-$\frac{3}{2}$ band in the rotationally-symmetric limit [31]. Using Eq. 5 we find that the gaps opened by these pairing states have nontrivial band dependence. This is most apparent in the A_{2u} case, which in the spin-$\frac{1}{2}$ band has fourteen nodes along the (100) and (111) and equivalent directions, whereas in the spin-$\frac{3}{2}$ band it only has six nodes along the the (100) directions [32]. These nodes result from the spin-momentum locking: along the (100) directions the A_{2u} state pairs electrons with helicity differing by ±2 which cannot be satisfied in either band, and hence implies purely interband pairing and a node in the intraband gap. On the other hand, along the (111) direction the A_{2u} state pairs electrons with helicity differing by ±3, and so it only opens a gap in the spin-$\frac{3}{2}$ band. In contrast, the A_{1u} state pairs electrons with the same helicity, and hence it opens a full gap in both bands. Further details on these pairing states are provided in the appendix B.

The response of the superconductivity to an applied Zeeman field displays major differences between the two bands. For a field applied along the z-axis, the averaged field-fitness function $\tilde{F}^{(a)}_h = \langle\tilde{F}^{(a)}_{h,\boldsymbol{k}}\rangle_a$ is plotted in Fig. 1(a) and (b) as a function of β_2/β_1 for the A_{1u} and A_{2u} states, respectively. In the spin-$\frac{1}{2}$ band, the nonzero value of $\tilde{F}^{(a)}_h$ indicates that a magnetic field is partially pair-breaking for both states; in the spin-$\frac{3}{2}$ band, however, the field is almost completely pair-breaking for the A_{1u} state, whereas the A_{2u} state is almost insensitive to its effects. These results are only weakly dependent upon the ratio β_2/β_1, and become exact in the rotationally-symmetric limit. This behaviour is reflected in the susceptibility, as shown in Fig. 1(c) and (d): in the spin-$\frac{3}{2}$ band the Pauli contribution to the susceptibility is completely suppressed for the A_{1u} state, whereas we see no change in the susceptibility for the A_{2u} state. In contrast, in both cases there is moderate suppression of the susceptibility in the spin-$\frac{1}{2}$ band. Likewise, as shown in Fig. 1(e) and (f), in the spin-$\frac{3}{2}$ band the A_{1u} state is Pauli-limited whereas the A_{2u} state is only limited by orbital effects.

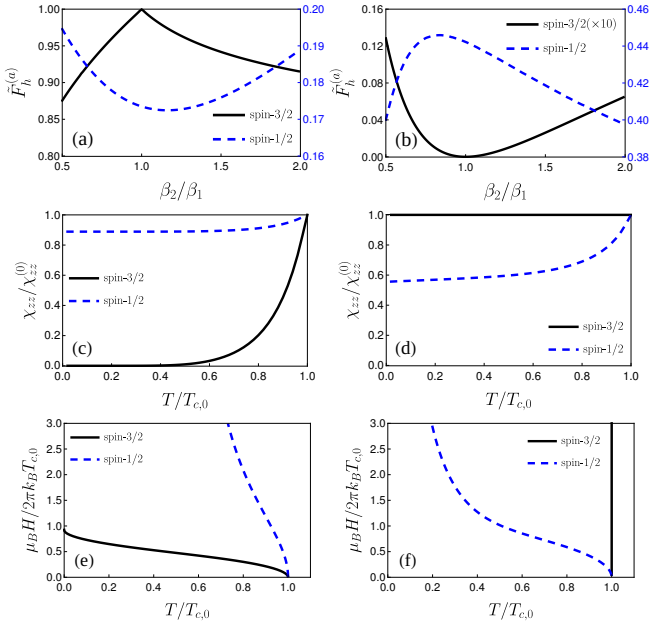


Figure 1. Comparison of A_{1u} and A_{2u} states. (a), (b): Normalized field-fitness $\tilde{F}^{(a)}_h$ on the spin-3/2 (black solid line, $\mu = -20$meV) and spin-1/2 (blue dashed line, $\mu = 20$meV) band Fermi surface for A_{1u} (a) and A_{2u} (b) pairing. (c), (d): Pauli susceptibility as a function of temperature at $\beta_2 = \beta_1$ for A_{1u} (c) and A_{2u} (d) pairing. (e), (f) Upper critical field excluding orbital effects for each band at $\beta_2 = \beta_1$ for A_{1u} (e) and A_{2u} (f) pairing. In all plots we take $\alpha = 20(a/\pi)^2$eV, $\beta_1 = -15(a/\pi)^2$eV.

The remarkable response to a magnetic field can be understood in the rotationally-symmetric limit in terms of the helicity quantum number. Projected onto the spin-$\frac{3}{2}$ band, the A_{1u} state pairs electrons with the same helicity whereas the A_{2u} state pairs electrons with opposite helicity. In the projection of the Zeeman Hamiltonian only the $J^z_{\boldsymbol{k}}$ operator has nonzero matrix elements, and so the energy shift of the state $|\sigma\rangle_{\boldsymbol{k}}$ is $\sigma\mathbf{h}\cdot\hat{\boldsymbol{k}}$. Since the A_{2u} state pairs electrons which have the same Zeeman shift, it does not experience pair-breaking; in contrast, the A_{1u} state pairs electrons with opposite Zeeman shift, and the pair-breaking is maximal. The situation in the spin-$\frac{1}{2}$ band is more complicated, since helicity is not a good quantum number for the projected Zeeman Hamiltonian, and the A_{2u} state has both equal- and opposite-helicity pairing matrix elements. This gives the intermediate values of $\tilde{F}^{(a)}_h$ for the spin-$\frac{1}{2}$ band. Although this argument is only rigorously valid in the rotationally-symmetric limit, the plot of $\tilde{F}^{(a)}_h$ in Fig. 1(a) and (b) indicates that it remains valid more generally.

Conclusions. In this paper we have developed a basis-independent framework to understand the interplay of

superconductivity and symmetry-breaking perturbations in a multiband system. Using a generic minimal model, we have shown that that coupling of orbital and spin degrees of freedom typically reduces the effect of the perturbation via the appearance of an effective g-factor Eq. 8. Moreover, the pair-breaking effect of this perturbation can be formulated in terms of the field-fitness function Eq. 9. Together, these quantities control the suppression of the critical temperature by the perturbation, and in the case of a Zeeman field determine the magnetic susceptibility below the critical temperature. To illustrate these effects, we have examined p-wave pairing of effective spin-$\frac{3}{2}$ electrons with normal state described by the Luttinger-Kohn model. The characteristic spin-momentum locking in this model leads to the remarkable result that in the spin-$\frac{3}{2}$ band the triplet A_{1u} state is strongly suppressed by a Zeeman field, whereas the septet A_{2u} state is largely immune to it, giving dramatically different behaviour in the upper critical field and the spin susceptibility.

Acknowledgements D.C.C. and P.M.R.B were supported by the Marsden Fund Council from Government funding, managed by Royal Society Te Apārangi. D.F.A. was supported by the U.S. Department of Energy, Office of Basic Energy Sciences, Division of Materials Sciences and Engineering, under Award No. DE-SC0021971.

[1] S. Ran, C. Eckberg, Q.-P. Ding, Y. Furukawa, T. Metz, S. R. Saha, I.-L. Liu, M. Zic, H. Kim, J. Paglione, and N. P. Butch, Nearly ferromagnetic spin-triplet superconductivity, Science **365**, 684 (2019).

[2] S. Khim, J. F. Landaeta, J. Banda, N. Bannor, M. Brando, P. M. R. Brydon, D. Hafner, R. Küchler, R. Cardoso-Gil, U. Stockert, A. P. Mackenzie, D. F. Agterberg, C. Geibel, and E. Hassinger, Field-induced transition within the superconducting state of $CeRh_2As_2$, Science **373**, 1012 (2021).

[3] D. Aoki, A. Nakamura, F. Honda, D. Li, Y. Homma, Y. Shimizu, Y. J. Sato, G. Knebel, J.-P. Brison, A. Pourret, D. Braithwaite, G. Lapertot, Q. Niu, M. Vališka, H. Harima, and J. Flouquet, Unconventional superconductivity in heavy fermion UTe_2, Journal of the Physical Society of Japan **88**, 043702 (2019).

[4] D. H. Nguyen, A. Sidorenko, M. Taupin, G. Knebel, G. Lapertot, E. Schuberth, and S. Paschen, Superconductivity in an extreme strange metal, Nature Communications **12**, 4341 (2021).

[5] V. P. Mineev and K. V. Samokhin, *Introduction to Unconventional Superconductivity* (Gordon and Breach Science Publishers, 1999).

[6] M. Sigrist, Introduction to unconventional superconductivity, AIP Conference Proceedings **789**, 165 (2005).

[7] M. Shimozawa, S. K. Goh, R. Endo, R. Kobayashi, T. Watashige, Y. Mizukami, H. Ikeda, H. Shishido, Y. Yanase, T. Terashima, T. Shibauchi, and Y. Matsuda, Controllable rashba spin-orbit interaction in artificially engineered superlattices involving the heavy-fermion superconductor $cecoin_5$, Phys. Rev. Lett. **112**, 156404 (2014).

[8] T. Watanabe, T. Yoshida, and Y. Yanase, Odd-parity superconductivity by competing spin-orbit coupling and orbital effect in artificial heterostructures, Phys. Rev. B **92**, 174502 (2015).

[9] D. C. Cavanagh, T. Shishidou, M. Weinert, P. M. R. Brydon, and D. F. Agterberg, Nonsymmorphic symmetry and field-driven odd-parity pairing in $Cerh_2as_2$, Phys. Rev. B **105**, L020505 (2022).

[10] Y.-M. Xie, B. T. Zhou, and K. T. Law, Spin-orbit-parity-coupled superconductivity in topological monolayer WTe_2, Phys. Rev. Lett. **125**, 107001 (2020).

[11] X. Zhang, Q. Liu, J.-W. Luo, A. J. Freeman, and A. Zunger, Hidden spin polarization in inversion-symmetric bulk crystals, Nature Physics **10**, 387 (2014).

[12] M. Smidman, M. B. Salamon, H. Q. Yuan, and D. F. Agterberg, Superconductivity and spin–orbit coupling in non-centrosymmetric materials: a review, Reports on Progress in Physics **80**, 036501 (2017).

[13] S. J. Youn, M. H. Fischer, S. H. Rhim, M. Sigrist, and D. F. Agterberg, Role of strong spin-orbit coupling in the superconductivity of the hexagonal pnictide srptas, Phys. Rev. B **85**, 220505 (2012).

[14] T. Yoshida, M. Sigrist, and Y. Yanase, Pair-density wave states through spin-orbit coupling in multilayer superconductors, Phys. Rev. B **86**, 134514 (2012).

[15] O. Vafek and A. V. Chubukov, Hund Interaction, Spin-Orbit Coupling, and the Mechanism of Superconductivity in Strongly Hole-Doped Iron Pnictides, Phys. Rev. Lett. **118**, 087003 (2017).

[16] A. Ramires and M. Sigrist, Identifying detrimental effects for multiorbital superconductivity: Application to Sr_2RuO_4, Phys. Rev. B **94**, 104501 (2016).

[17] H. G. Suh, H. Menke, P. M. R. Brydon, C. Timm, A. Ramires, and D. F. Agterberg, Stabilizing even-parity chiral superconductivity in sr_2ruo_4, Phys. Rev. Research **2**, 032023 (2020).

[18] P. M. R. Brydon, L. Wang, M. Weinert, and D. F. Agterberg, Pairing of $j = 3/2$ Fermions in Half-Heusler Superconductors, Phys. Rev. Lett. **116**, 177001 (2016).

[19] L. Savary, J. Ruhman, J. W. F. Venderbos, L. Fu, and P. A. Lee, Superconductivity in three-dimensional spin-orbit coupled semimetals, Phys. Rev. B **96**, 214514 (2017).

[20] S. Kobayashi, A. Bhattacharya, C. Timm, and P. M. R. Brydon, Bogoliubov fermi surfaces from pairing of emergent $j = \frac{3}{2}$ fermions on the pyrochlore lattice, Phys. Rev. B **105**, 134507 (2022).

[21] J. W. F. Venderbos, L. Savary, J. Ruhman, P. A. Lee, and L. Fu, Pairing States of Spin-$\frac{3}{2}$ Fermions: Symmetry-Enforced Topological Gap Functions, Phys. Rev. X **8**, 011029 (2018).

[22] D. Kim, T. Sato, S. Kobayashi, and Y. Asano, Spin susceptibility of a $j = 3/2$ superconductor, arXiv:2206.14994 (2022).

[23] A. Ramires, D. F. Agterberg, and M. Sigrist, Tailoring T_c by symmetry principles: The concept of superconducting fitness, Phys. Rev. B **98**, 024501 (2018).

[24] P. M. R. Brydon, D. F. Agterberg, H. Menke, and

C. Timm, Bogoliubov Fermi surfaces: General theory, magnetic order, and topology, Phys. Rev. B **98**, 224509 (2018).
[25] A. A. Abrikosov, Calculation of critical indices for zero-gap semiconductors, Sov. Phys. JETP **39**, 709 (1974).
[26] L. Fu and E. Berg, Odd-Parity Topological Superconductors: Theory and Application to $Cu_xBi_2Se_3$, Phys. Rev. Lett. **105**, 097001 (2010).
[27] Y. Yanase, Nonsymmorphic Weyl superconductivity in UPt_3 based on E_{2u} representation, Phys. Rev. B **94**, 174502 (2016).
[28] D. F. Agterberg, T. Shishidou, J. O'Halloran, P. M. R. Brydon, and M. Weinert, Resilient nodeless d-wave superconductivity in monolayer fese, Phys. Rev. Lett. **119**, 267001 (2017).
[29] S. Ilić, J. S. Meyer, and M. Houzet, Enhancement of the upper critical field in disordered transition metal dichalcogenide monolayers, Phys. Rev. Lett. **119**, 117001 (2017).
[30] M. D. E. Denys and P. M. R. Brydon, Origin of the anomalous hall effect in two-band chiral superconductors, Phys. Rev. B **103**, 094503 (2021).
[31] J. M. Link and I. F. Herbut, p-wave superconductivity in Luttinger semimetals, Phys. Rev. B **105**, 134522 (2022).
[32] J. W. F. Venderbos, L. Savary, J. Ruhman, P. A. Lee, and L. Fu, Pairing States of Spin-$\frac{3}{2}$ Fermions: Symmetry-Enforced Topological Gap Functions, Phys. Rev. X **8**, 011029 (2018).

Appendix A: General results on the effect of broken symmetry

1. The Green's function

In the absence of symmetry-breaking perturbations, the Green's function is

$$G\left(\boldsymbol{k}, i\omega_n\right) = \sum_{a=\pm} \frac{1}{i\omega_n - \xi_{a,\boldsymbol{k}}} \mathcal{P}_{a,\boldsymbol{k}}, \tag{A1}$$

where $\mathcal{P}_{a,\boldsymbol{k}}$ projects onto band a at wavevector $\boldsymbol{k}$, given explicitly by

$$\mathcal{P}_{a,\boldsymbol{k}} = \frac{\mathbb{1} + a\hat{\varepsilon}_{\boldsymbol{k}} \cdot \vec{\gamma}}{2} = \frac{1}{2}\left[\mathbb{1} + a\frac{\bar{\mathcal{H}}_{0,\boldsymbol{k}}}{|\vec{\varepsilon}_{\boldsymbol{k}}|}\right]. \tag{A2}$$

We now consider the addition of the symmetry-breaking perturbation. Assuming that $h_{\boldsymbol{k}} \ll |\vec{\epsilon}_{\boldsymbol{k}}|$, i.e. the mixing between the unperturbed bands is negligible, we can approximate the Green's function by

$$G\left(\boldsymbol{k}, i\omega_n\right) = \sum_{a,b=\pm} \frac{1}{i\omega_n - \xi_{a,b,\boldsymbol{k}}} \mathcal{P}_{a,b,\boldsymbol{k}}, \tag{A3}$$

where $\xi_{a,b,\boldsymbol{k}} = \xi_{a,\boldsymbol{k}} + b\tilde{g}_{a,\boldsymbol{k}} h_{\boldsymbol{k}}$ and the projection operator is defined

$$\mathcal{P}_{a,b,\boldsymbol{k}} = \frac{1}{4}\left(\mathbb{1} + a\frac{\bar{\mathcal{H}}_{0,\boldsymbol{k}}}{|\vec{\varepsilon}_{\boldsymbol{k}}|}\right)\left(\mathbb{1} + ab\frac{\left\{\bar{\mathcal{H}}_{0,\boldsymbol{k}}, \mathcal{H}_{h,\boldsymbol{k}}\right\}}{2\tilde{g}_{a,\boldsymbol{k}} h\,|\vec{\varepsilon}_{\boldsymbol{k}}|}\right) \tag{A4}$$

This expression is valid to lowest order in $h_{\alpha,\boldsymbol{k}}/|\vec{\varepsilon}_{\boldsymbol{k}}|$, which is equivalent to ignoring interband corrections.

2. The linearized gap equation

The pairing potential Δ_0 is determined by self-consistent solution of the gap equation

$$\Delta_0 = -V_0\beta \sum_{i\omega_n,\boldsymbol{k}} \mathrm{Tr}\{\tilde{\Delta}_{\boldsymbol{k}}^{\dagger} F\left(\boldsymbol{k}, i\omega_n\right)\}, \tag{A5}$$

where $F(\boldsymbol{k}, i\omega_n)$ is the anomalous Green's function and V_0 is the pairing interaction. Ignoring interband pairing, just below the critical temperature the anomalous Green's function in the presence of symmetry-breaking perturbations can be approximated by

$$F\left(\boldsymbol{k}, i\omega_n\right) = \sum_{a,b,b'} \frac{\mathcal{P}_{a,b,\boldsymbol{k}} \Delta_{\boldsymbol{k}} \mathcal{P}^{T}_{a,b',-\boldsymbol{k}}}{\left(i\omega_n - \xi_{a,b,\boldsymbol{k}}\right)\left(i\omega_n + \xi_{a,b',\boldsymbol{k}}\right)}. \tag{A6}$$

Inserting this into the gap equation we obtained the linearized form

$$-\frac{1}{V_0} = \beta \sum_{i\omega_n,\boldsymbol{k}} \sum_{a,b,b'} \frac{\mathrm{Tr}\{\tilde{\Delta}_{\boldsymbol{k}}^{\dagger} \mathcal{P}_{a,b,\boldsymbol{k}} \tilde{\Delta}_{\boldsymbol{k}} \mathcal{P}_{a,\bar{b}',\boldsymbol{k}}\}}{\left(i\omega_n - \xi_{a,b,\boldsymbol{k}}\right)\left(i\omega_n + \xi_{a,b',\boldsymbol{k}}\right)}. \tag{A7}$$

Performing the sums over Matsubara frequency and momentum gives Eq. 10 after the zero-field result is subtracted.

3. Spin susceptibility

The static long-wavelength paramagnetic i-axis susceptibility can be divided into an intraband Pauli contribution and an interband van Vleck contribution

$$\chi_{ii} = \sum_a \{\chi_{ii,aa} + \chi_{ii,a\bar{a}}\}. \tag{A8}$$

In the normal state these terms are given by

$$\chi^{(N)}_{ii,aa} = \sum_{\boldsymbol{k}} \frac{\mu_B^2 \bar{\chi}^{(N)}_{ii,aa}\left(\boldsymbol{k}\right)}{8\,|\vec{\varepsilon}_{\boldsymbol{k}}|^2} \mathrm{Tr}\{|\left\{S_i, \bar{\mathcal{H}}_{0,\boldsymbol{k}}\right\}|^2 \mathcal{P}_{a,\boldsymbol{k}}\} \tag{A9}$$

$$\chi^{(N)}_{ii,a\bar{a}} = \sum_{\boldsymbol{k}} \frac{\mu_B^2 \bar{\chi}^{(N)}_{ii,a\bar{a}}\left(\boldsymbol{k}\right)}{16\,|\vec{\varepsilon}_{\boldsymbol{k}}|^2} \mathrm{Tr}\{|[S_i, \bar{\mathcal{H}}_{0,\boldsymbol{k}}]|^2\}. \tag{A10}$$

Here S_i is the spin operator in the i direction. In spin-$\frac{1}{2}$ materials this is given by $S_i = \tau_0 \otimes \sigma_i$, whereas $S_i = J_i$ for effective spin-$\frac{3}{2}$ materials. The traces in these expression encode the effect of the spin-orbital texture of the band electron states; note the appearance of the effective g-factor in the Pauli contribution. This modulates the Lindhard function

$$\bar{\chi}^{(N)}_{ii,aa'}\left(\boldsymbol{k}\right) = \lim_{\boldsymbol{q}\to\boldsymbol{0}} \frac{n_F\left(\xi_{a,\boldsymbol{k}+\boldsymbol{q}}\right) - n_F\left(\xi_{a',\boldsymbol{k}}\right)}{\xi_{a,\boldsymbol{k}+\boldsymbol{q}} - \xi_{a',\boldsymbol{k}}} \tag{A11}$$

where n_F is the Fermi-Dirac function.

The Pauli susceptibility is significantly modified below the critical temperature due to the opening of the superconducting gap. Moreover, it develops an anomalous contribution due to the pairing

$$\chi^{(A)}_{ii,aa} = \sum_{\boldsymbol{k}} \frac{\mu_B^2 \bar{\chi}^{(A)}_{ii,aa}(\boldsymbol{k})}{256\,|\vec{\varepsilon}_{\boldsymbol{k}}|^4} \mathrm{Tr}\{(|\{\{S_i, \bar{\mathcal{H}}_{0,\boldsymbol{k}}\}, \{\tilde{\Delta}_{\boldsymbol{k}}, \bar{\mathcal{H}}_{0,\boldsymbol{k}}\}\}|^2 - |[\{S_i, \bar{\mathcal{H}}_{0,\boldsymbol{k}}\}, \{\tilde{\Delta}_{\boldsymbol{k}}, \bar{\mathcal{H}}_{0,\boldsymbol{k}}\}]|^2)\mathcal{P}_{a,\boldsymbol{k}}\}. \tag{A12}$$

The modified Lindhard function appearing in this expression is

$$\bar{\chi}^{(A)}_{ii,aa'}(\boldsymbol{k}) = \lim_{\boldsymbol{q}\to\boldsymbol{0}} \frac{|\Delta_{0,\boldsymbol{k}+\boldsymbol{q}}|\,|\Delta_{0,\boldsymbol{k}}|}{E_{a,\boldsymbol{k}+\boldsymbol{q}} E_{a',\boldsymbol{k}}} \left\{ \frac{n_F(E_{a,\boldsymbol{k}+\boldsymbol{q}}) - n_F(E_{a',\boldsymbol{k}})}{E_{a,\boldsymbol{k}+\boldsymbol{q}} - E_{a',\boldsymbol{k}}} - \frac{1 - n_F(E_{a,\boldsymbol{k}+\boldsymbol{q}}) - n_F(E_{a',\boldsymbol{k}})}{E_{a,\boldsymbol{k}+\boldsymbol{q}} + E_{a',\boldsymbol{k}}} \right\}, \tag{A13}$$

where $E_{a,\boldsymbol{k}} = \sqrt{\xi^2_{a,\boldsymbol{k}} + |\Delta_{a,\boldsymbol{k}}|^2}$. The Lindhard function appearing in the "normal" contribution is also modified as

$$\begin{aligned}\bar{\chi}^{(N)}_{ii,aa'}(\boldsymbol{k}) = \lim_{\boldsymbol{q}\to\boldsymbol{0}} \frac{-\mu_B}{2} \Bigg\{ &\left[1 + \frac{\xi_{a,\boldsymbol{k}+\boldsymbol{q}}\xi_{a',\boldsymbol{k}}}{E_{a,\boldsymbol{k}+\boldsymbol{q}} E_{a',\boldsymbol{k}}}\right] \frac{n_F(E_{a,\boldsymbol{k}+\boldsymbol{q}}) - n_F(E_{a',\boldsymbol{k}})}{E_{a,\boldsymbol{k}+\boldsymbol{q}} - E_{a',\boldsymbol{k}}} \\ &+ \left[1 - \frac{\xi_{a,\boldsymbol{k}+\boldsymbol{q}}\xi_{a',\boldsymbol{k}}}{E_{a,\boldsymbol{k}+\boldsymbol{q}} E_{a',\boldsymbol{k}}}\right] \frac{1 - n_F(E_{a,\boldsymbol{k}+\boldsymbol{q}}) - n_F(E_{a',\boldsymbol{k}})}{E_{a,\boldsymbol{k}+\boldsymbol{q}} + E_{a',\boldsymbol{k}}} \Bigg\},\end{aligned} \tag{A14}$$

If the superconducting gap has even parity, the anomalous contribution to the Pauli susceptibility will exactly cancel the normal part as $T \to 0$. More generally any such cancellation depends sensitively on the spin-orbital texture and structure of the gap.

4. Broken inversion symmetry

In the main text we focus on the effect of a perturbation which breaks time-reversal symmetry. Our formalism, can also account for inversion symmetry-breaking perturbations such as a weak antisymmetric spin-orbit coupling. In the presence of an inversion symmetry breaking perturbation, the critical temperature is given by Eq. 10, with the field-fitness replaced by

$$\tilde{F}^{(a)}_{h,\boldsymbol{k}} = \frac{\mathrm{Tr}\{|[\{\bar{\mathcal{H}}_{0,\boldsymbol{k}}, \tilde{\Delta}_{\boldsymbol{k}}\}, \{\bar{\mathcal{H}}_{0,\boldsymbol{k}}, \mathcal{H}_{h,\boldsymbol{k}}\}]|^2 \mathcal{P}_{a,\boldsymbol{k}}\}}{2\mathrm{Tr}\{|\{\bar{\mathcal{H}}_{0,\boldsymbol{k}}, \mathcal{H}_{h,\boldsymbol{k}}\}|^2 \mathcal{P}_{a,\boldsymbol{k}}\}\mathrm{Tr}\{|\{\bar{\mathcal{H}}_{0,\boldsymbol{k}}, \tilde{\Delta}_{\boldsymbol{k}}\}|^2 \mathcal{P}_{a,\boldsymbol{k}}\}}. \tag{A15}$$

The key difference compared to Eq. 9 of the main text is that the numerator involves the commutator of the anticommutators, as opposed to the anticommutator of the anticommutators. It can be straightforwardly shown that $\tilde{F}^{(a)}_{h,\boldsymbol{k}} = 0$ for all even-parity superconductors, reflecting the fact that the intraband potential of these states always pairs time-reversed partners.

Appendix B: $J = \frac{3}{2}$ superconductors

1. Spherical limit

In the spherical limit the Luttinger-Kohn Hamiltonian takes the form

$$H = \alpha|\boldsymbol{k}|^2 \hat{1}_4 + \beta(\boldsymbol{k}\cdot\mathbf{J})^2. \tag{B1}$$

We observe that the Hamiltonian has two doubly-degenerate bands corresponding to $\langle \boldsymbol{k}\cdot\mathbf{J}\rangle = \pm\frac{3}{2}|\boldsymbol{k}|$ and $\langle \boldsymbol{k}\cdot\mathbf{J}\rangle = \pm\frac{1}{2}|\boldsymbol{k}|$. We will refer to these two bands as the spin-$\frac{3}{2}$ and spin-$\frac{1}{2}$ bands, respectively. A natural choice of basis for these bands is the "helical" basis

$$\{|\tfrac{3}{2}\rangle_{\boldsymbol{k}},\ |-\tfrac{3}{2}\rangle_{\boldsymbol{k}}\}, \qquad \{|\tfrac{1}{2}\rangle_{\boldsymbol{k}},\ |-\tfrac{1}{2}\rangle_{\boldsymbol{k}}\} \tag{B2}$$

where $\boldsymbol{k}\cdot\mathbf{J}|\sigma\rangle_{\boldsymbol{k}} = \sigma|\boldsymbol{k}||\sigma\rangle_{\boldsymbol{k}}$. Note that the operator $\boldsymbol{k}\cdot\hat{\mathbf{J}}$ is invariant under time-reversal, and so the "helicity" σ is *not* a pseudospin index. Expressed in terms of the z-spin eigenstates we have

$$\begin{aligned}|\tfrac{3}{2}\rangle_{\boldsymbol{k}} &= e^{-3i\phi}\cos^3(\tfrac{\theta}{2})|\tfrac{3}{2}\rangle + \sqrt{3}e^{-2i\phi}\cos^2(\tfrac{\theta}{2})\sin(\tfrac{\theta}{2})|\tfrac{1}{2}\rangle \\ &\quad + \sqrt{3}e^{-i\phi}\cos(\tfrac{\theta}{2})\sin^2(\tfrac{\theta}{2})|-\tfrac{1}{2}\rangle + \sin^3(\tfrac{\theta}{2})|-\tfrac{3}{2}\rangle \end{aligned} \tag{B3}$$

$$\begin{aligned}|\tfrac{1}{2}\rangle_{\boldsymbol{k}} &= -\sqrt{3}e^{-3i\phi}\sin(\tfrac{\theta}{2})\cos^2(\tfrac{\theta}{2})|\tfrac{3}{2}\rangle \\ &\quad + \frac{1}{2}e^{-2i\phi}[-1 + 3\cos(\theta)]\cos(\tfrac{\theta}{2})|\tfrac{1}{2}\rangle \\ &\quad + \frac{1}{2}e^{-i\phi}[1 + 3\cos(\theta)]\sin(\tfrac{\theta}{2})|-\tfrac{1}{2}\rangle \\ &\quad + \sqrt{3}\sin^2(\tfrac{\theta}{2})\cos(\tfrac{\theta}{2})|-\tfrac{3}{2}\rangle \end{aligned} \tag{B4}$$

$$\begin{aligned}|-\tfrac{1}{2}\rangle_{\boldsymbol{k}} &= \sqrt{3}e^{-3i\phi}\sin^2(\tfrac{\theta}{2})\cos(\tfrac{\theta}{2})|\tfrac{3}{2}\rangle \\ &\quad - \frac{1}{2}e^{-2i\phi}[1 + 3\cos(\theta)]\sin(\tfrac{\theta}{2})|\tfrac{1}{2}\rangle \\ &\quad + \frac{1}{2}e^{-i\phi}[-1 + 3\cos(\theta)]\cos(\tfrac{\theta}{2})|-\tfrac{1}{2}\rangle \\ &\quad + \sqrt{3}\sin(\tfrac{\theta}{2})\cos^2(\tfrac{\theta}{2})|-\tfrac{3}{2}\rangle \end{aligned} \tag{B5}$$

$$\begin{aligned}|-\tfrac{3}{2}\rangle_{\boldsymbol{k}} &= -e^{-3i\phi}\sin^3(\tfrac{\theta}{2})|\tfrac{3}{2}\rangle + \sqrt{3}e^{-2i\phi}\sin^2(\tfrac{\theta}{2})\cos(\tfrac{\theta}{2})|\tfrac{1}{2}\rangle \\ &\quad - \sqrt{3}e^{-i\phi}\sin(\tfrac{\theta}{2})\cos^2(\tfrac{\theta}{2})|-\tfrac{1}{2}\rangle + \cos^3(\tfrac{\theta}{2})|-\tfrac{3}{2}\rangle \end{aligned} \tag{B6}$$

where (ϕ, θ) are the angular coordinates defined by the direction of $\boldsymbol{k}$. The helicity index reverses under inversion

$\mathcal{I}$ but is preserved under time-reversal $\mathcal{T}$:

$$\mathcal{I}|\pm\tfrac{3}{2}\rangle_{\boldsymbol{k}} = |\mp\tfrac{3}{2}\rangle_{-\mathbf{k}}\,, \quad \mathcal{I}|\pm\tfrac{1}{2}\rangle_{\boldsymbol{k}} = |\mp\tfrac{1}{2}\rangle_{-\mathbf{k}}\,, \tag{B7}$$

$$\mathcal{T}|\pm\tfrac{3}{2}\rangle_{\boldsymbol{k}} = \mp e^{3i\phi}|\pm\tfrac{3}{2}\rangle_{-\mathbf{k}}\,, \quad \mathcal{T}|\pm\tfrac{1}{2}\rangle_{\boldsymbol{k}} = \pm e^{3i\phi}|\pm\tfrac{1}{2}\rangle_{-\mathbf{k}}\,, \tag{B8}$$

Because of the momentum-dependent quantization axis, it is useful to define the momentum-dependent angular-momentum operators

$$J_z^{\boldsymbol{k}} = \hat{\mathbf{k}}\cdot\mathbf{J}\,, \quad J_\pm^{\boldsymbol{k}} = \left(\hat{\boldsymbol{\theta}}_{\boldsymbol{k}} \pm i\hat{\boldsymbol{\phi}}_{\boldsymbol{k}}\right)\cdot\mathbf{J} \tag{B9}$$

where $\hat{\boldsymbol{\theta}}_{\boldsymbol{k}} = \cos\phi\cos\theta\hat{\mathbf{x}} + \sin\phi\cos\theta\hat{\mathbf{y}} - \sin\theta\hat{\mathbf{z}}$ and $\hat{\boldsymbol{\phi}}_{\boldsymbol{k}} = -\sin\phi\hat{\mathbf{x}} + \cos\phi\hat{\mathbf{y}}$ are the canonical spherical-coordinate unit vectors in the directions perpendicular to $\hat{\boldsymbol{k}}$.

2. The Zeeman field

We include a Zeeman field in Hamiltonian as

$$H_{\mathrm{Z}} = g\mu_B\mathbf{h}\cdot\mathbf{J}$$

To understand the effect of the spin-orbit coupling we now re-express this in terms of the momentum-dependent angular momentum operators:

$$H_{\mathrm{Z}}^{\boldsymbol{k}} = g\mu_B h\left[\hat{\mathbf{h}}\cdot\hat{\boldsymbol{k}}J_z^{\boldsymbol{k}} + \hat{\mathbf{h}}\cdot\left(\hat{\boldsymbol{\theta}}_{\boldsymbol{k}} + i\hat{\boldsymbol{\phi}}_{\boldsymbol{k}}\right)J_+^{\boldsymbol{k}} + \hat{\mathbf{h}}\cdot\left(\hat{\boldsymbol{\theta}}_{\boldsymbol{k}} - i\hat{\boldsymbol{\phi}}_{\boldsymbol{k}}\right)J_-^{\boldsymbol{k}}\right]\,. \tag{B10}$$

Note that for $\boldsymbol{k}$ in the direction of the applied field, only the first term is present, and the Zeeman field is diagonal in the helical basis. Conversely, for $\boldsymbol{k}$ perpendicular to the applied field, only the second and third terms are present, and the Zeeman field couples the helical states with helicity σ differing by ±1.

3. The pairing states

a. *The p-wave A_{1u} state*

The p-wave A_{1u} has

$$\tilde{\Delta}(\boldsymbol{k}) = \boldsymbol{k}\cdot\mathbf{J} = |\boldsymbol{k}|J_z^{\boldsymbol{k}} \tag{B11}$$

Since $\tilde{\Delta}(\boldsymbol{k})$ is proportional to $J_z^{\boldsymbol{k}}$, and the helicity is preserved under time-reversal, this pairs states with the same helicity. This implies that in the spherical limit the A_{1u} state corresponds to purely intraband pairing.

b. *The p-wave A_{2u} state*

The p-wave A_{2u} has the pair potential

$$\begin{aligned}
\tilde{\Delta}(\boldsymbol{k}) &= \sum_{i=x,y,z} k_i[J_{i+1}J_iJ_{i+1} - J_{i+2}J_iJ_{i+2}] \\
&= |\boldsymbol{k}|\Bigg(\frac{1}{32}[6\cos2\phi\sin2\theta + 3i(3+\cos2\theta)\sin\theta\sin2\phi]J_+^{\boldsymbol{k}}J_+^{\boldsymbol{k}}J_+^{\boldsymbol{k}} \\
&\quad + \frac{1}{32}[6\cos2\phi\sin2\theta - 3i(3+\cos2\theta)\sin\theta\sin2\phi]J_-^{\boldsymbol{k}}J_-^{\boldsymbol{k}}J_-^{\boldsymbol{k}} \\
&\quad + \frac{1}{8}[4\cos2\phi\cos2\theta + i(1+3\cos2\theta)\cos\theta\sin2\phi]J_+^{\boldsymbol{k}}J_z^{\boldsymbol{k}}J_+^{\boldsymbol{k}} \\
&\quad + \frac{1}{8}[4\cos2\phi\cos2\theta - i(1+3\cos2\theta)\cos\theta\sin2\phi]J_-^{\boldsymbol{k}}J_z^{\boldsymbol{k}}J_-^{\boldsymbol{k}} \\
&\quad - \frac{1}{128}\left[2\cos2\phi\sin2\theta + i(1+3\cos2\theta)\sin\theta\sin2\phi\right](7J_+^{\boldsymbol{k}} - 20J_z^{\boldsymbol{k}}J_+^{\boldsymbol{k}}J_z^{\boldsymbol{k}}) \\
&\quad - \frac{1}{128}\left[2\cos2\phi\sin2\theta - i(1+3\cos2\theta)\sin\theta\sin2\phi\right](7J_-^{\boldsymbol{k}} - 20J_z^{\boldsymbol{k}}J_-^{\boldsymbol{k}}J_z^{\boldsymbol{k}})\Bigg)
\end{aligned} \tag{B12}$$

Although very complicated compared to the A_{1u} case, we observe that the pair potential never pairs electrons with the same helicity, since it always involves operators which change the helicity. That is, projected into the band basis, the pair potential only pairs the states $|\sigma\rangle_{\boldsymbol{k}}$ and $|-\sigma\rangle_{-\mathbf{k}}$. Moreover, we have the following special cases:

- along the crystal axes $(\phi,\theta) = (0,\frac{\pi}{2})$, $(\frac{\pi}{2},\frac{\pi}{2})$, $(\phi,0)$, only the coefficients of $J_\pm^{\boldsymbol{k}}J_z^{\boldsymbol{k}}J_\pm^{\boldsymbol{k}}$ are nonzero, i.e. the pairing potential pairs states with helicity differing by ±2. This cannot be satisfied in either band, and so the intraband gap develops a node.
- along the crystal body diagonals $(\phi,\theta) = (\pm\frac{\pi}{4}, \pm\arctan\sqrt{2})$ only the coefficients of $J_\pm^{\boldsymbol{k}}J_\pm^{\boldsymbol{k}}J_\pm^{\boldsymbol{k}}$ are nonzero, i.e. the pairing potential pairs states with helicity differing by ±3, i.e. there is only pair-

ing in the spin-$\frac{3}{2}$ band. Consequently the gap in the spin-$\frac{1}{2}$ band has nodes.